International Journal of High-Rise Buildings
Vol 1, No 2, June 2012, 107-116

International Journal of
High-Rise Buildings
www.ctbuh.org

Numerical Analysis of Convective Heat and Mass Transfer around Human Body under Strong Wind

Cong Li and Kazuhide Ito†

Interdisciplinary Graduate School of Engineering Science, Kyushu University, Fukuoka, 816-8580, Japan

Abstract

The overarching objective of this study is to predict the convective heat transfer around a human body under forced strong airflow conditions assuming a strong wind blowing through high-rise buildings or an air shower system in an enclosed space. In this study, computational fluid dynamics (CFD) analyses of the flow field and temperature distributions around a human body were carried out to estimate the convective heat transfer coefficient for a whole human body assuming adult male geometry under forced convective airflow conditions between 15 m/s and 25 m/s. A total of 45 CFD analyses were analyzed with boundary conditions that included differences in the air velocity, wind direction and turbulence intensity. In the case of approach air velocity U_{in} = 25 m/s and turbulent intensity TI = 10%, average convective heat transfer coefficient was estimated at approximately 100 W/m^2/K for the whole body, and strong dependence on air velocity and turbulence intensity was confirmed. Finally, the formula for the mean convective heat transfer coefficient as a function of approaching average velocity and turbulence intensity was approximated by using the concept of equivalent steady wind speed (U_{eq}).

Keywords: Forced convective flow, Convective heat transfer coefficient, Virtual Manikin, Computational fluid dynamics

1. Introduction

Occasionally, a human body will be exposed to a forced convective airflow, for example, a strong wind blowing through high-rise buildings, a severe tropical storm or typhoon, a strong wind during mountain climbing, or an air-shower system in enclosed space.

From the viewpoint of ensuring the safety of people and reducing the effects of disasters, control of strong winds is crucial in the design of residential spaces. Considering the physiology of human beings, forced strong convective airflow would be the dominant parameter of heat loss from the human body; on the other hand, this indicates the efficiency of desorption or detachment of contaminant on the surface of the human body, especially in an air-shower system in industrial application. Generally, one of the critical physical parameters to express the transportation between a body surface (solid phase) and the atmospheric air around a human body (fluid phase) is convective heat transfer coefficient in thermodynamics or mass transfer around a human body.

As stated above, the convective heat transfer coefficient becomes one of the critical parameters to estimate thermal sensation/comfort; therefore, many researchers have investigated and reported detailed information on the convective heat transfer coefficient based on numerical simulation and chamber experiment, especially under low-air-velocity conditions, that is, less than 1 m/s. Various researchers, such as Seppanen et al., de Dear et al., Ichihara et al., Watanabe et al., and Kuwahara et al., conducted precise experiments using a thermal manikin with real geometry and reported the predictive formulas of convective heat transfer coefficient (CHTC; α_c) of the whole body and each body segment (Seppanen et al., 1972; de Dear et al., 1997; Ichihara et al., 1997; Watanabe et al., 2008; Kuwahara et al., 2001). The experimental parameter used in these studies to identify convective heat transfer coefficient for a human body was mainly average air velocity approaching the thermal manikin, and the prediction formulas were a simple function of average velocity. Lee et al. experimentally estimated the convective heat transfer coefficient of the thermal manikin with change in air velocity and turbulence intensity (Lee et al., 1991). According to their results, the convective heat transfer coefficient increased significantly with the increase of turbulence intensity under conditions in which the airflow was over 0.3 m/s.

Concerning numerical work for the identification of convective heat transfer coefficient for the human body, there has been plenty of research on CFD simulation using the computer simulated person (CSP), numerical thermal manikin and Virtual Manikin (VM) with the purpose of determining detailed characteristics of heat transfer, which are difficult to obtain from experiments. Murakami and Kato's research group was the first developer of a numerical thermal manikin, and has reported the

†Corresponding author: Kazuhide Ito
Tel: +81-92-583-7628; Fax: +81-92-583-7627
E-mail: ito@kyudai.jp

numerical simulation results for the micro-climate formed around the human body and heat loss as a function of air velocity by a CFD method (Murakami et al., 1997, 1999, 2000). Yang et al. investigated the convective heat transfer coefficient for a human body under stagnant flow conditions by a numerical thermal manikin and CFD approach, and reported the validation of their results by using an experimental thermal manikin in the same scenario as the numerical analysis (Yang et al., 2004).

In order to provide an applicable convective heat transfer coefficient, especially in an outdoor context, Ono et al. reported the estimation results of both experimental and CFD analyses (Ono et al., 2006). However, most of the researchers have focused on relatively low-velocity cases (several m/s or less, maximum approximately 5 m/s in the case of Ono et al.), and there have been no reports targeting high-velocity conditions, for example, above 10 m/s.

In this study, computational fluid dynamics (CFD) analyses of the flow field and temperature distributions around a human body were carried out to estimate the convective heat transfer coefficient for the whole human body assuming an adult male geometry under forced convective flow conditions from 15 m/s to 25 m/s.

The overarching objective of this study is to provide detailed information on the convective heat transfer coefficient for the whole human body under forced strong wind by a CFD approach and to propose simple prediction formulas of convective heat transfer coefficient as functions of the average approaching wind velocity, turbulent intensity and wind direction to a human body for the design of urban wind environments or air shower systems, among others.

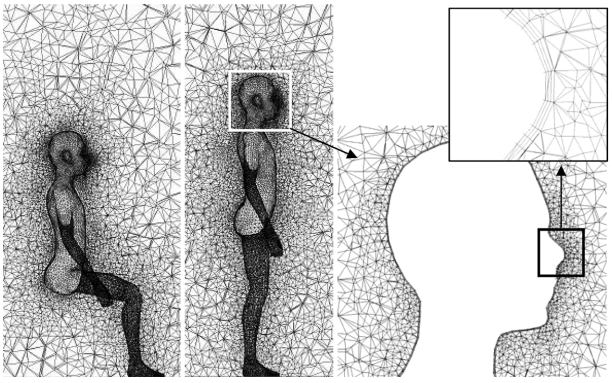


Figure 1. Grid design around virtual manikin.

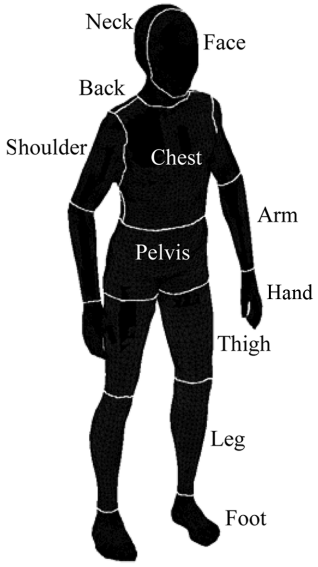


Figure 2. Segments of the body.

2. Virtual Manikin

In order to analyze the micro-climate around a human body in an indoor environment, a series of Virtual Manikins have been developed by our research group (Ito and Hotta, 2006). We have already developed and reported a total of six kinds of Virtual Manikins: three types of human scales of a seven-year-old child model (Child Model), an adult male model (Male Model) and an adult female model (Female Model), and two types of postures: standing model and seated model. Detailed information on the Virtual Manikins developed by our group is provided elsewhere (Ito and Hotta, 2006). Virtual Manikins imitate the standard Japanese body proportions (7-year-old child, adult male and adult female). The outlines of the human body are drawn using posture generation software (POSER 4.0J, Curious Labs Inc.) and the data are then read out in DXF format. The overall shape of the human body is then adjusted by using three-dimensional

Table 1. Surface area of the segments of the Virtual Manikin

Segment	Standing male model
Area of whole body [m^2]	1.745
Volume of whole body [m^3]	0.064
Height of body [m]	1.736
Smallest surface mesh size [mm^2]	0.469
Largest surface mesh size [mm^2]	425.013
The number of surface meshes	44,974
Area of left and right foot [m^2]	0.048
Area of left and right leg [m^2]	0.111
Area of left and right thigh [m^2]	0.151
Area of left and right hand [m^2]	0.038
Area of left and right arm [m^2]	0.071
Area of left and right shoulder [m^2]	0.074
Area of pelvis [m^2]	0.265
Area of chest [m^2]	0.190
Area of back [m^2]	0.127
Area of face [m^2]	0.062
Area of neck [m^2]	0.086

CAD software (Vector Works and A&A Co. Ltd.). The final geometry of the Virtual Manikins and computational grids are made using a publicly available commercial mesh generator (GRIDGEN V15, VINAS Co. Ltd.). The hands and feet of the Virtual Manikin are simplified in consideration of the computational load for the CFD analysis. An example of the grid arrangement around a Virtual Manikin is shown in Fig. 1. The surface of each Virtual Manikin is divided into 17 segments (see Fig. 2), corresponding approximately to the original divisions of the thermal manikin (Madsen, 1976).

In this study, the Virtual Manikin for a standing adult male model was used for integrated analysis of CFD and Virtual Manikin to predict convective heat transfer around a human body. Essential information for the Virtual Manikin for a standing adult male model is given in Table 1.

3. Outline of Numerical Analysis

Fig. 3 shows the outline of target space for numerical simulation with the Virtual Manikin. The standing Virtual Manikin was arranged at the center of the analytical room of dimensions $x = 3.0$ m, $y = 3.0$ m and $z = 3.0$ m. Uniform flow boundary conditions were generated in the analytical room, and the uniform supply inlet velocity U_{in} was controlled at three levels: 15.0 m/s, 20.0 m/s and 25.0 m/s. The turbulent intensity of supply inlet air flow was controlled at five levels; 10%, 20%, 30%, 40% and 50%. The temperature of the supply inlet was maintained constant at $T_{in} = 303$ K and the walls surrounding the Virtual Manikin, except for the supply inlet and exhaust outlet, were assumed to be isothermal at $T_{wall} = 303$ K, whereas the surface temperature of the Virtual Manikin $T_{sk} = 306.7$ K was fixed on the basis of the boundary conditions from previous CFD research (Ono et al., 2006).

The total number of computational cells in the analytical space was set up from approximately one to two million cells in accordance with the approaching wind velocity. The surface mesh reproduced the complex geometry of the human body shape arranged with a triangular surface mesh. To solve the boundary layer around the Virtual Manikin, at least a few layers of prism cells were created on the surface of the Virtual Manikin with an equal height between layers and continuously at least four layers of prism cells were allocated with an equal height of less than 1.0 mm. The tetra-meshes were then arranged from the outside of the boundary layer to the other side walls in the analytical model room. The rationale behind the two-region setup is that the unstructured grids ensure reasonable accuracy for a given number of grid points and stretching towards the side walls. Under these numerical conditions, the wall units (y^+) that express the dimensionless normal distance from the surface approximately met the requirement of 1.0 over the whole surface of the Virtual Manikin.

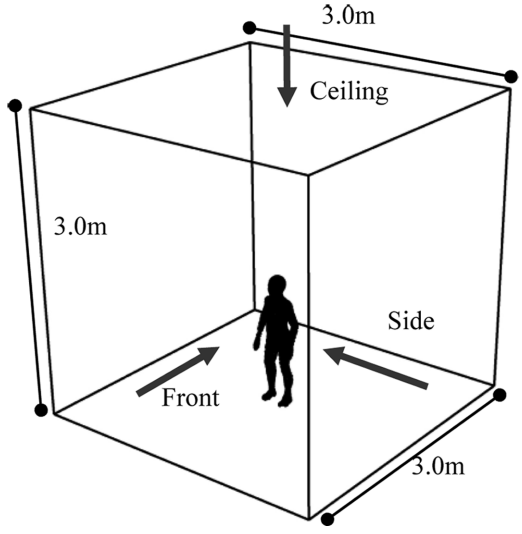


Figure 3. Analytical domain with a Virtual Manikin and approach flow directions.

3.1. CFD analysis of flow and temperature distribution around Virtual Manikin

Analysis of the flow and temperature fields in the analytical domain with the Virtual Manikin located in the center of the floor was carried out by numerical analysis based on CFD. The commercial CFD code (ANSYS/Fluent 12.0, ANSYS Co. Ltd.) was used to calculate the flow and heat transfer around the human body. The flow fields were analyzed three-dimensionally using the SST k-ω model (Menter et al., 2003) in the steady-state condition. The SIMPLE algorithm was used with the QUICK scheme for the convection terms, and a second-order center difference scheme was used for the others. The no-slip condition was adopted as the wall surface boundary condition for the velocity and hence the flow pattern and detailed temperature gradient inside the viscous sub-layer could be precisely analyzed. The skin surface temperatures of the Virtual Manikin were fixed at a constant value. Table 2 shows the details of the

Table 2. Numerical and boundary conditions

Turbulence model	SST k-ω model (3-dimensional calc.)
Scheme	Convection term: QUICK
Inflow boundary	Area of Supply Inlet: 3.0 m × 3.0 m, $U_{in} = 15.0, 20.0, 25.0$ m/s, $T_{in} = 303$ K, $TI = 10, 20, 30, 40, 50\%$ $k_{in} = 3/2 \times (U_{in} \times 0.01 \bullet TI)^2$, $\varepsilon_{in} = C_\mu \times k_{in}^{3/2}/l_{in}$, $C_\mu = 0.09$, $l_{in} = 3.0$ m
Inflow direction	Front, Side, Upper (In view of Virtual Manikin)
Outflow boundary	U_{out} = Free slip, k_{out} = Free slip, ε_{out} = Free slip
Wall treatment	Velocity: No slip, $k\|_{wall}$: No slip Temperature: $T_{wall} = 303$ K (=Const.)
Surface treatment of manikin	Velocity: No slip, $k\|_{wall}$: No slip Temperature: $T_{sk} = 306.7$ K (=Const.)

numerical and boundary conditions.

Concerning the prediction accuracy of the SST k-ω model for heat transfer analysis in high-velocity conditions, we have already conducted validation work with a wind tunnel experiment and also CFD under the same boundary conditions of experimental scenarios and have reported reasonable consistency of the prediction results of the SST k-ω model and wind tunnel results (Li et al., 2012). We have also investigated the prediction accuracy of two types of turbulent models: SST k-ω model and low Re type k-ε model (Abe- Kondoh- Nagano model), that compared the results of wind tunnel experiment with thermal manikin. As for the CFD simulation around human body under high velocity condition, we have already confirmed and reported that SST k-ω model that integrate in control mechanism to excessive production of turbulent kinetic energy *k* showed reasonable and acceptable prediction results (Li et al., 2012).

3.2. Cases analyzed

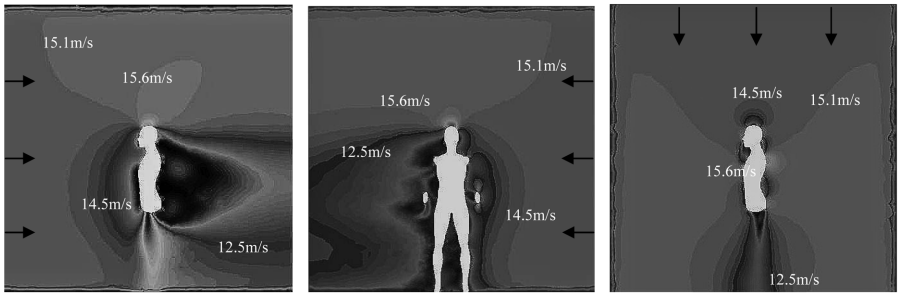
In this analysis, the analytical parameters were taken as the inflow air velocity, turbulence intensity and wind direction. The uniform and constant air velocity U_{in} was set at three levels (15.0, 20.0 and 25.0 m/s). The turbulence intensity was set at five levels (10, 20, 30, 40, and 50%). The wind directed at the standing Virtual Manikin was set in three directions: towards the face of the Virtual Manikin, from the side, which represents cross wind, and from the ceiling, with perpendicular and downward flow inside an air shower system. All these boundary conditions were combined and CFD analysis was carried out on totally 45 cases.

3.3. Calculation of the mean convective heat transfer coefficient

The Virtual Manikin used in this analysis was divided into 17 segments as shown in Fig. 2, and hence the mean convective heat transfer coefficient for each segment could be calculated. In this study, we focused on the general phenomenon of heat and mass transfer around a human body under forced strong wind for the design and assessment of urban wind environment; the mean convective heat transfer coefficient was calculated for the whole body using the area-weighted average of each computational surface segment. The convective heat transfer coefficient [W/m^2/K] for each computational segment of the Virtual Manikin was estimated from the following equation:

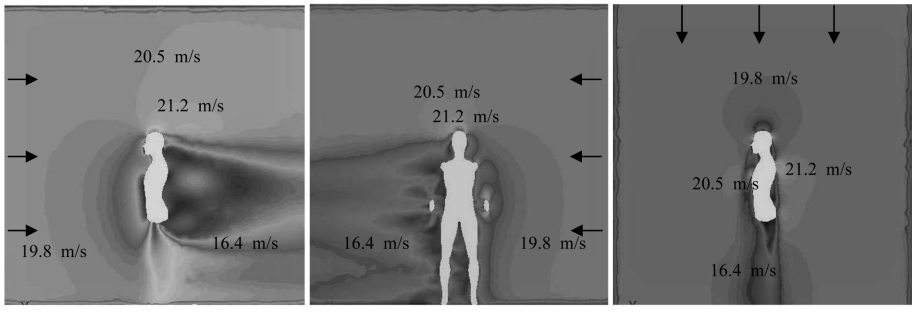
$$\alpha_c = \frac{Q_c}{(T_{sk} - T_{ref})} \tag{1}$$

Here, Q_c is the convective heat transfer rate [W/m^2] calculated by a flow field analysis based on the SST k-ω model and the energy transport equation, T_{sk} is the skin surface temperature [K] of the Virtual Manikin (T_{sk} = 306.7) and T_{ref} is the inflow air temperature [K] used as



(1) Approach from the front (2) Approach from the right side (3) Approach from the ceiling

(a) Flow Field (U_{in}=15 m/s, TI=10%)



(4) Approach from the front (5) Approach from the right side (6) Approach from the ceiling

(b) Flow Field (U_{in}=20 m/s, TI=10%)

Figure 4. Flow field around the Virtual Manikin.

the reference temperature ($T_{in} = T_{ref} = 303$). Since the surface temperatures of the walls and skin surface were given as fixed values, no analysis of the radiative heat transfer was carried out.

4. Results of Numerical Simulation

4.1. Flow fields

The prediction results of flow fields around the Virtual Manikin are shown in Fig. 4. Here, the results under the conditions of ($U_{in} = 15$ m/s and $TI = 10\%$) and ($U_{in} = 20$ m/s and $TI = 10\%$) are denoted as representative. The flow fields were analyzed by the SST k-ω model. Here, the results for three wind directions: approach from the front, approach from the left side of the Virtual Manikin and approach from the ceiling, are shown.

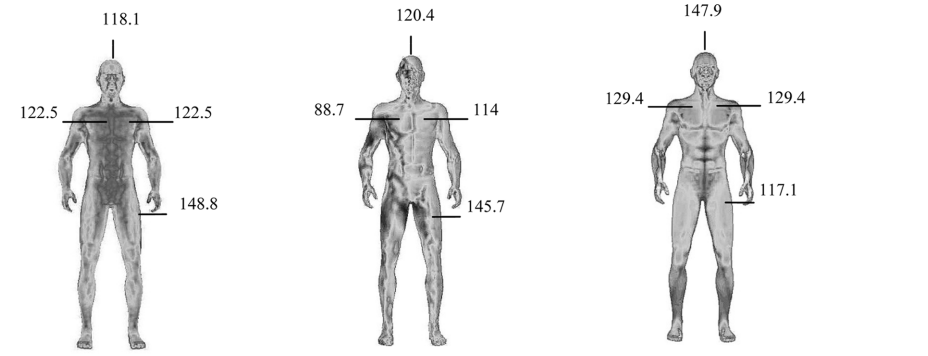
In the case of wind approach from the front of the Virtual Manikin (Fig. 4(1)), approach flow impinged on the front face of the human body and subsequently the airflow was broken by the human body; hence, a stagnant flow region was formed behind the human body. In the case of wind approach from the right side of the Virtual Manikin (Fig. 4(2)), the flow pattern was separated by the human body and the formation of a stagnant region in the wake flow side was almost the same as that in the case of wind approach from the front. In the case of approach flow from the ceiling (Fig. 4(3)), an approximately uniform flow field around the human body was generated because the effective surface area of the human body against the approach flow was relatively small compared with those in other conditions.

The flow patterns and distributions around human body in case of ($U_{in} = 20$ m/s, $TI = 10\%$) were almost analogous to that in ($U_{in} = 15$ m/s, $TI = 10\%$).

4.2. Convective heat transfer coefficients (CHTC)

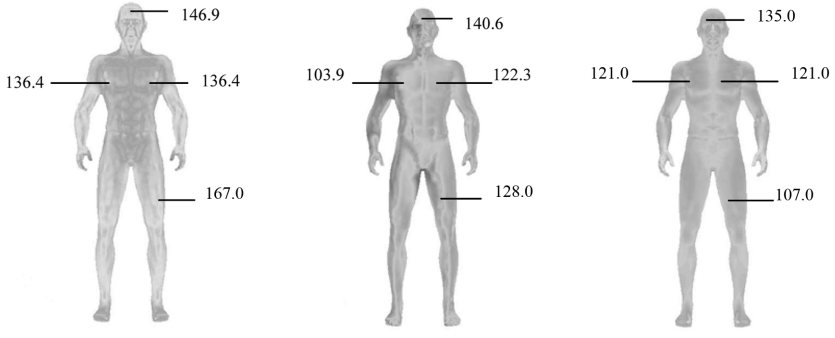
Prediction results for distributions of convective heat transfer coefficient (CHTC) on the surface of the Virtual Manikin are shown in Fig. 5, which take the conditions of $U_{in} = 25$ m/s and $TI = 10\%$, $U_{in} = 15$ m/s, $TI = 30\%$ as example. Unit of CHTC in these figures is [W/m^2/K].

Non-uniform distribution of CHTC on the surface of the human body was confirmed and the value of CHTC became larger in the high-velocity region around the human body, while it was lower in the stagnant region. The local maximum value of CHTC surpassed 150 W/m^2/K in this analysis.



(1) Approach from the front (2) Approach from the left side (3) Approach from the ceiling

(a) CHTC distributions (U_{in}=25 m/s, TI=10%)



(1) Approach from the front (2) Approach from the left side (3) Approach from the ceiling

(b) CHTC distributions (U_{in}=15 m/s, TI=30%)

Figure 5. Distributions of convective heat transfer coefficient on the surface of the Virtual Manikin.

4.3. Relationship between convective heat transfer coefficient and average velocity, turbulent intensity

Fig. 6 shows the relationship between CHTC and average approach wind velocity, turbulent intensity. The approximately linear or logarithmic relationship between the increase of CHTC and that of average wind velocity was confirmed under the conditions of strong wind from 15 to 25 m/s. The CHTC was also increased with an increase in turbulent intensity.

4.4. Prediction formulas of convective heat transfer coefficient around human body under strong wind

Here, we deal with prediction formulas of convective heat transfer coefficient under the airflow conditions of U_{in} from 15 to 25 m/s and of *TI* from 10 to 50%. In this study, two types of prediction formulas are proposed: (i) simplified formulas based on equivalent steady wind speed (U_{eq}) and (ii) the formulas using polynomial approximation as functions of average approach wind velocity (U_{in}) and turbulence intensity (*TI*).

Hunt et al. proposed the concept of equivalent steady wind speed (U_{eq}) as follows (Hunt et al., 1976):

$$U_{eq} = U(1 + PF \times TI/100) \tag{2}$$

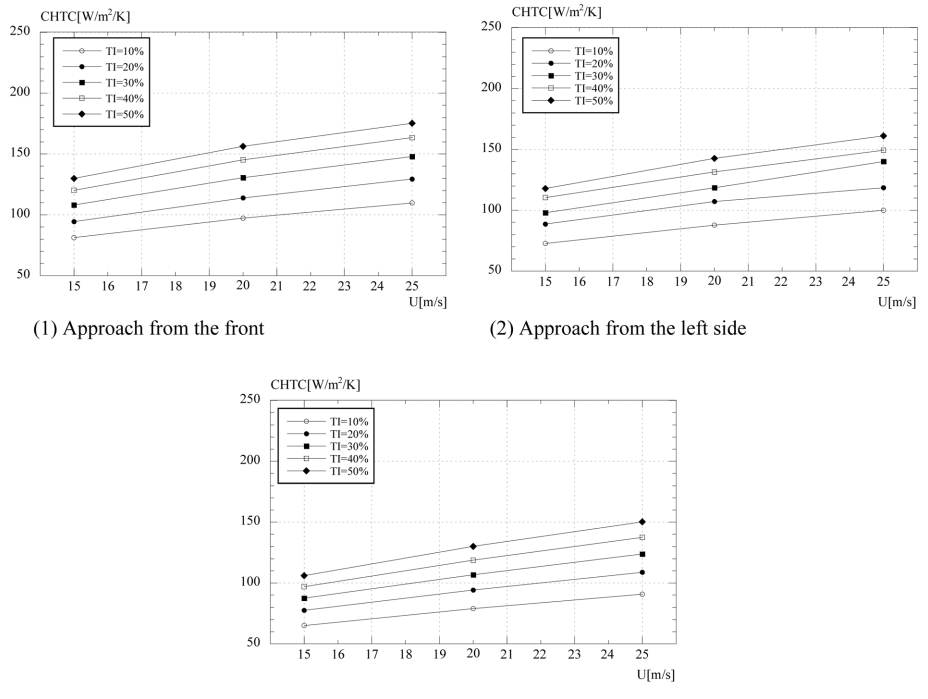
This equivalent steady wind speed (U_{eq}) is a frequently used concept for assessment of urban wind environment. The *PF* in Eq. (2) is called peak factor and indicates the ratio of peak wind velocity and average wind velocity as a function of standard deviation. Various values of *PF*, for example, from 1.0 to 4, have been proposed. In other words, equivalent steady wind speed (U_{eq}) denotes the maximum instantaneous wind speed U_{max} under the condition of assumed *PF*. Hunt et al. have proposed a *PF* of approximately 3 as a representative peak factor in outdoor wind environments; therefore, the equivalent steady wind speeds (U_{eq}) are identified by using $PF = 3$ in this study.

The calculations of CHTC and U_{eq} for different wind directions are shown in Fig. 7. The relationship of linear or power law could be confirmed between the two parameters. Here, the relationship between equivalent steady wind speed (U_{eq}) and convective heat transfer coefficient (CHTC) is expressed by a power law-type formula as shown in Eq. (3).

$$\alpha_c = a U_{eq}^{b} \tag{3}$$

The model coefficients '*a*' and '*b*' in Eq. (3) were estimated by the method of least squares and are summarized in Table 3 for three approach wind directions. As seen in Fig. 7, the value of CHTC for the whole human body follows well for the power law formulation of U_{eq}. Although the value of CHTC became large in the case of wind approach from the front-way, for the increasing rate of CHTC, the case with wind approach from the ceiling (top) became the maximum.

Predictive formulas of polynomial approximation of the CHTC as a function of mean air velocity *U* [m/s] and turbulence intensity *TI* [%] was proposed as the following



(1) Approach from the front

(2) Approach from the left side

(3) Approach from the ceiling

Figure 6. Relationship between the CHTC, average wind velocity, turbulence intensity.

equation:

$$a_c = a_0 + a_1 \times U + a_2 \times (U \cdot TI) - a_3 \times (U^2 \cdot TI) \quad (4)$$

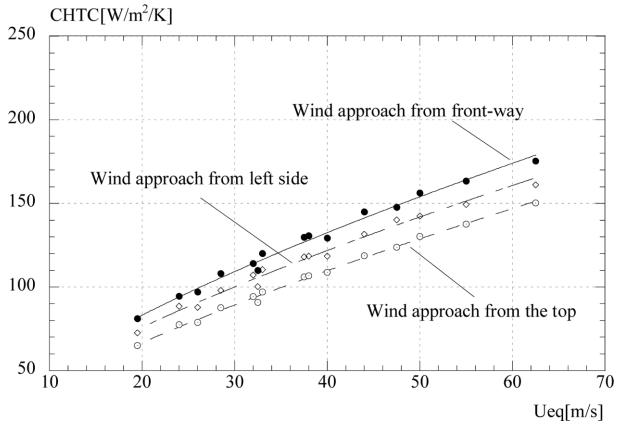


Figure 7. CHTC and equivalent velocity U_{eq} for different wind directions.

The least squares regression result was given in Table 4, and the predictive curves was then graphically plotted in Fig. 8, including three wind approach directions. For every fitted curve its correlation coefficient R^2 is less than 0.97. Meanwhile, it should be noted that this paper only investigated three types of velocities (15, 20, 25 m/s), few variable terms can be added into this polynomial shape predictive formula but their impact on the prediction result is minimal. And therefore we proposed a simplified formula as Eq. (4).

5. Discussion

Assuming analogy between heat transfer and mass transfer, Nusselt number (Nu) and Sherwood number (Sh) are expressed by using dimensionless number as follows:

$$Nu = C \cdot Re^m \cdot Pr^n \quad (5)$$

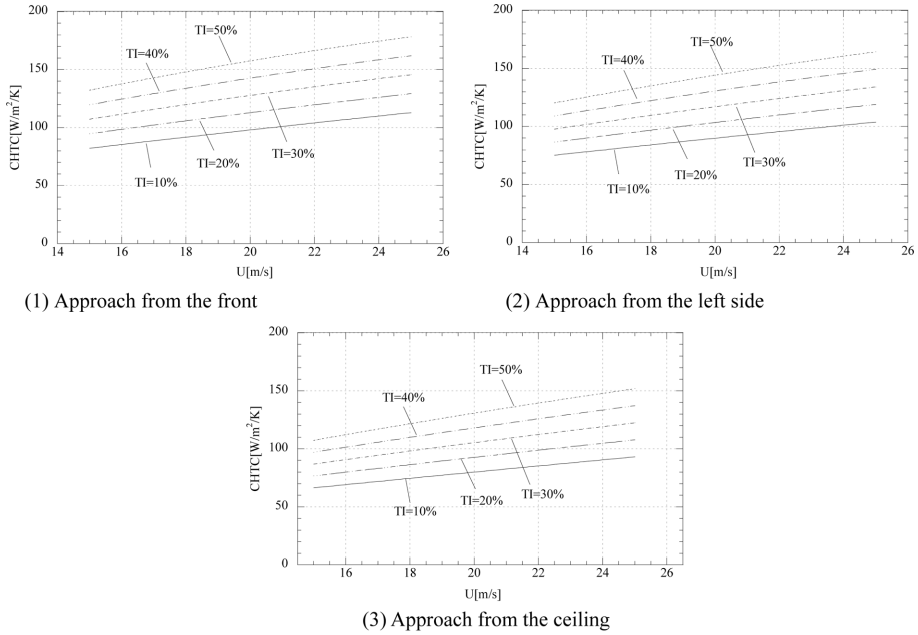
$$Sh = C \cdot Re^m \cdot Sc^n \quad (6)$$

Table 3. Prediction formulas of CHTC of the whole body as a function of U_{eq} ($\alpha_c = aU_{eq}^b$, $U_{eq} = U(1 + PF \times TI/100)$)

Wind direction	(1) Wind approach from the front		(2) Wind approach from the left side		(3) Wind approach from the ceiling	
Coefficients of the prediction formulas	a	b	a	b	a	b
	11.110	0.672	9.809	0.683	7.738	0.719

Table 4. Prediction formulas of CHTC of the whole body as a function of U [m/s] and TI [%] ($a_c = a_0 + a_1 \times U + a_2 \times (U \cdot TI) - a_3 \times (U^2 \cdot TI)$)

Wind direction	(1) Wind approach from the front	(2) Wind approach from the left side	(3) Wind approach from the ceiling
Prediction formulas of CHTC of the whole body [1.745 m²]	$a_c = 29.397 + 2.684 \times U + 11.045 \times (U \cdot TI) - 0.18 \times (U^2 \cdot TI)$	$a_c = 26.983 + 2.469 \times U + 9.682 \times (U \cdot TI) - 0.145 \times (U^2 \cdot TI)$	$a_c = 22.739 + 2.224 \times U + 8.25 \times (U \cdot TI) - 0.095 \times (U^2 \cdot TI)$



(1) Approach from the front

(2) Approach from the left side

(3) Approach from the ceiling

Figure 8. Prediction of CHTC as a function of average velocity and turbulence intensity.

Eq. (7) is introduced by dividing both sides of Eqs. (5) and (6), and subsequently Eq. (8) is obtained from the definitions of Nusselt number (*Nu*) and Sherwood number (*Sh*).

$$\frac{Nu}{Sh}=\left(\frac{Pr}{Sc}\right)^{n} \tag{7}$$

$$\frac{Nu}{Sh}=\frac{\alpha_c}{\alpha_D}\frac{D}{\alpha}\frac{1}{\rho c_p} \tag{8}$$

Eq. (9) is derived from Eqs. (7) and (8). Finally, the relationship between convective heat transfer coefficient and mass transfer coefficient is expressed through the Lewis number.

$$\alpha_c=\alpha_D\cdot\rho c_p\cdot Le^{1-n} \tag{9}$$

$$Le=\frac{\alpha}{D} \tag{10}$$

The Lewis number of gaseous matter is known as approximately 1.

Here, the mass transfer coefficient assuming vapor transport is estimated by using the Lewis relationship expressed in Eqs. (9) and (10). The order of mass transfer coefficients was 5.17×10^{-2} m/s in the case of U_{in} = 15 m/s and *TI* = 10% under the condition of approach flow from the ceiling, 6.27×10^{-2} m/s in the case of U_{in} = 20 m/s and *TI* = 10% under the condition of approach flow from the ceiling, and 11.96×10^{-2} m/s in the case of U_{in} = 25 m/s and *TI* = 50% under the condition of approach flow from the ceiling.

Fig. 9 shows the relationship between the mass transfer coefficient converted from CHTC, average wind velocity and turbulent intensity. These figures in Fig. 9 are analogous to that in Fig. 6.

6. Conclusions

Here, the convective heat transfer coefficient (CHTC) around the human body was analyzed by CFD with the SST k-ω model and the prediction formulas of CHTC as functions of average wind velocity and turbulence intensity under strong wind conditions from 15 m/s to 25 m/s was proposed. The findings of this study are as follows:

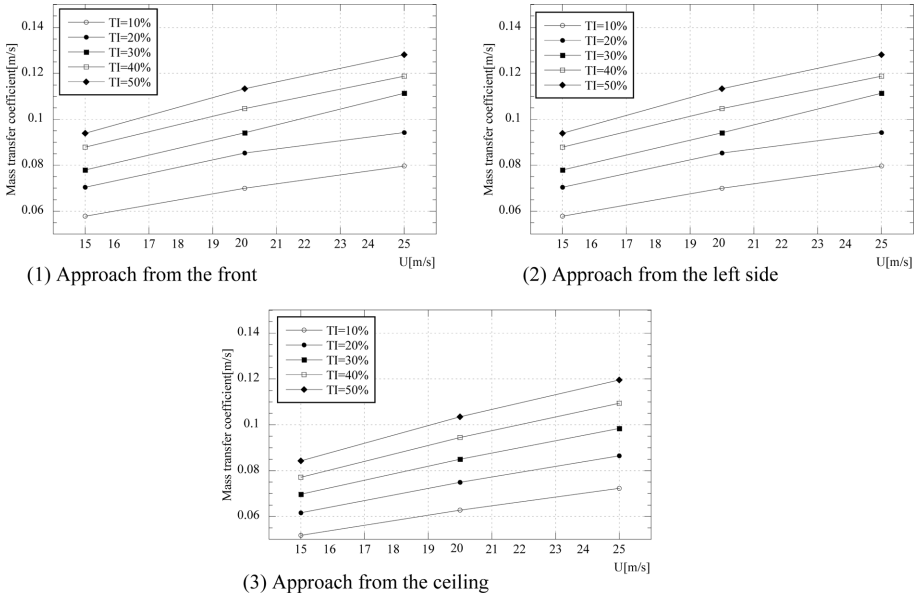
(1) The average convective heat transfer coefficient around the human body became larger in accordance with the increase of approach wind speed and turbulence intensity. The approximately power law-type relationships between an increase in the average convective heat transfer coefficient around the human body and that in air velocity were confirmed.

(2) The CHTC for the whole human body showed dependence on wind direction, and the CHTC in the case of flow approach from the front was approximately 9 to 19% larger than those for the other wind directions.

(3) Assuming analogy between heat transfer and mass transfer, the mass transfer coefficient in the case of water vapor transfer from the human body surface was assumed. The range of mass transfer coefficients under strong convective flow (U_{in} from 15 to 25 m/s) was identified from 5×10^{-2} m/s to 10.0×10^{-2} m/s, and these values of mass transfer coefficients were approximately 1/10 of those in typical indoor environmental conditions.

Acknowledgements

Dr. Eunsu Lim provided valuable suggestions on this research, for which the authors are deeply appreciative. This research was partly supported by a Grant-in-Aid for Scientific Research (JSPS KAKENHI for Young Scien-



(1) Approach from the front

(2) Approach from the left side

(3) Approach from the ceiling

Figure 9. Relationship between the mass transfer coefficient, average wind velocity, turbulence intensity.

tists (S), 21676005). The author would like to express special thanks to the funding source.

Appendix A

The transport equations of turbulent kinetic energy k and local scale vorticity ω (=ε/k) of SST k-ω model are as follows:

$$\frac{\partial \rho k}{\partial t}+\overline{U_i}\frac{\partial \rho k}{\partial x_i}=\min\left(\mu_t\left(\frac{\partial \overline{U_i}}{\partial x_j}+\frac{\partial \overline{U_j}}{\partial x_i}\right)\frac{\partial \overline{U_i}}{\partial x_j},10\rho\beta^* k\omega\right)$$

$$+\frac{\partial}{\partial x_j}\left\{\left(\mu+\frac{\mu_t}{\sigma_k}\right)\frac{\partial k}{\partial x_j}\right\}-\rho\beta^* k\omega$$

$$\frac{\partial \rho \omega}{\partial t}+\overline{U_i}\frac{\partial \rho \omega}{\partial x_i}=\rho\alpha\left(\frac{\partial \overline{U_i}}{\partial x_j}+\frac{\partial \overline{U_j}}{\partial x_i}\right)\frac{\partial \overline{U_i}}{\partial x_j}+\frac{\partial}{\partial x_j}\left\{\left(\mu+\frac{\mu_t}{\sigma_\varepsilon}\right)\frac{\partial \omega}{\partial x_j}\right\}$$

$$-\rho\beta\omega^2+2(1-F_1)\sigma_{\omega,2}\frac{1}{\omega}\frac{\partial k}{\partial x_j}\frac{\partial \omega}{\partial x_j}$$

The production term of turbulent kinetic energy k in the SST k-ω model was modified and incorporated a mechanism that controls the excessive production of k and hence the SST k-ω model could be applicable to the prediction of flow and convective heat transfer around complicated geometry, for example, a human body, under a strong wind. The authors have already reported the prediction accuracy of the SST k-ω model for convective heat transfer coefficient under strong convective flow conditions by using the experimental results in a wind tunnel under the same conditions as CFD (Li et al., 2012).

Appendix B

The definitions of dimensionless number in Eqs. (5) and (6) are as follows:

$$Gr=\frac{g\beta\Delta T\cdot Ln^3}{\nu^2},\ Nu=\frac{\alpha_c x}{\lambda},\ Pr=\frac{\nu}{\alpha},\ Ra=Pr\cdot Gr,$$

$$Re=\frac{U\cdot x}{\nu},\ Sh=\frac{\alpha_D\cdot x}{D},\ Sc=\frac{\nu}{D}$$

Here, α is thermal diffusivity [m^2/s], α_c is convective heat transfer coefficient [W/m^2/K], α_D is mass transfer coefficient [m/s], D is diffusion coefficient [m^2/s], c_p is specific heat at constant pressure of air [J/kg/K], ρ is air density [kg/m^3], Ln is representative length scale of natural convection [m], λ is thermal conductivity [W/m/K], x is representative length scale [m], ν is dynamic viscosity [m^2/s], g is acceleration due to gravity [m/s^2], U is representative velocity [m/s], T is temperature difference [K], and β is thermal expansion coefficient [1/K].

References

ANSYS (2009) ANSYS Fluent 12.1 Theory Guide.

de Dear, R. J., Arens, E. A., Hui, Z., and Oguro, M. (1997) "Convective and radiative heat transfer coefficient for individual human body segment", *International Journal of Biometeorology*, 40(3), pp. 141~156.

Fanger, P. O. (1970) Thermal comfort, Copenhagen, Danish Technical Press.

Ichihara, M., Saito, M., Nishihara, M., and Tanabe, S. (1997) "Measurement of convective and radiative heat transfer coefficients of standing and sitting human body by using a Thermal Manikin", *Journal of Architecture, Planning and Environmental Engineering, Architectural Institute of Japan*, 501, pp. 45~51. (In Japanese)

Ito, K. and Hotta, T. (2006) "Development of Virtual Manikins and its grid library for CFD analysis", *Transaction of SHASE (The Society of Heating, Air-Conditioning and Sanitary Engineers of Japan)*, 113, pp. 27~34. (In Japanese)

Kuwabara, K., Mochida, T., Kondoh, M., and Matsunaga, K. (2001) "Measurement of man's convective heat transfer coefficient by using a thermal manikin in the middle wind velocity region", *Journal of Human and Living Environment*, 8(1,2), pp. 27~32. (In Japanese)

Lee, C., Melikov, A. K., and Homma, H. (1991) "An experimental study on convective heat transfer coefficient distribution on Thermal Manikin by air flow with varisou velocities and turbulence intensities", *Journal of Architecture, Planning and Environmental Engineering, Architectural Institute of Japan*, 429, pp. 25~31 (In Japanese)

Li, C., Lim, E., and Ito, K. (2012) Development of wind decontamination system Part 1 - Measurement of convective heat transfer coefficient of human body in forced convective flowfield", *Transaction of SHASE (The Society of Heating, Air-Conditioning and Sanitary Engineers of Japan)*, 183, pp. 47~57. (In Japanese)

Menter, F. R., Kuntz, M., and Langtry, R. (2003) "Ten years of experience with the SST turbulence model", In K. Hanjalic, Y. Nagano, and M. Tummers, editors, *Turbulence, Heat and Mass Transfer 4*, pp. 625~632. Begell House Inc.

Hunt, J. C. R., Poulton, E. C., and Mumford, J. C. (1976) "The effects of wind people; New criteria based on wind tunnel experiments", *Building and Environment*, 11, pp. 15~28.

Madsen, T. L. (1976) "Description of thermal mannequin for measuring the thermal insulating capacity of the clothing", Report No.48, Technical University of Denmark.

Murakami, S., Kato, S., and Zeng, J. (1997) "Flow and temperature fields around human body with various room air distribution, CFD study on computational thermal manikin Part 1", *ASHRAE Transactions*, 103, Part 1, pp. 3~15.

Murakami, S., Kato, S., Zeng, J., and Hayashi, T. (1999) "CFD analysis of wind environment around a human body", *Journal Wind Engineering and Industrial Aerodynamics*, 83, pp. 393~408.

Ono, T., Murakami, S., Ooka, R., Takahashi, T., Omori, T., and Saotome, T. (2006) "Evaluation of mean convective heat transfer coefficient of a human body in outdoor environment: Proposal of the formula for mean

convective heat transfer coefficient of a human body by means of wind tunnel and CFD analysis", *Journal of Environmental Engineering, Architectural Institute of Japan*, 601, pp. 9~14. (In Japanese)

Ozeki, Y., Hiramatsu, T., Konishi, M., Nakano, J., and Tanabe, S. (2002) "Convective heat transfer coefficient at skin surface of thermal manikin under solar radiation", *Journal of Architecture, Planning and Environmental Engineering, Architectural Institute of Japan*, 555, pp. 29~36. (In Japanese)

Sorensen, D. N. and Voigt, L. K. (2003) "Modeling flow and heat transfer around a seated human body by computational fluid dynamics", *Building and Environment*, 38(6), pp. 753~762.

Tanabe, S., Arens, E. A., Bauman, F. S., Zhang, H., and Madsen, T. L. (1994) "Evaluating thermal environments by using thermal manikin with controlled skin surface temperature", *ASHRAE Transactions*, 100(1), pp. 39~48.

Topp, C., Nielsen, P. V., and Sørensen, D. N. (2002) "Application of computer simulated persons in indoor environmental modeling", *ASHRAE Transactions*, 108(2), pp. 1084~1089.

Seppanen, O., McNall, P. E., Munson, D. M., and Sprague, C. H. (1972) "Thermal insulating values for typical indoor clothing ensembles", *ASHRAE. Transactions*, 78, pp. 120~130.

Watanabe, S., Horikoshi, T., Ishii, J., Uno, T., Kaneko, T., and Tomiya, A. (2008) "Effect on wind velocities and wind directions on forced convective heat transfer coefficients for human body by using Thermal Manikin", *Journal of Environmental Engineering, Architectural Institute of Japan*, 629, pp. 887~893. (In Japanese)

Wilcox, D. C. (1988) "Reassessment of the scale-determining equation for advanced turbulence models", *AIAA J.*, 26, pp. 1299.

Yang, J. H., Kato, S., Hayashi, T., and Murakami, S. (2004) "Measurement of convective heat transfer coefficients with using an experimental and computational Thermal Manikin in indoor environments", *Journal of Environmental Engineering, Architectural Institute of Japan*, 584, pp. 33~40. (In Japanese)